Bull Eng Geol Environ (2019) 78:1815–1827
https://doi.org/10.1007/s10064-017-1185-2

ORIGINAL PAPER

Influences of internal erosion on infiltration and slope stability

Lulu Zhang[1,2] · **Fang Wu**[1,2] · **Hua Zhang**[3] · **Lei Zhang**[1,2] · **Jie Zhang**[4]

Received: 19 June 2017 / Accepted: 20 October 2017 / Published online: 11 November 2017

Abstract Rainfall-induced slope failures in natural terrains are destructive natural disasters. Transport of fine particles may be induced by the rainwater seepage in a natural terrain slope comprising mixed coarse and fine particles. In this study, the interaction of internal erosion and infiltration in a soil slope is investigated. A coupled model of unsaturated flow and internal erosion is established. The effects of internal erosion on pore water pressure profiles and slope stability are studied. Parametric studies on erosion parameters and hydraulic parameters are conducted. The results of the numerical example show that internal erosion occurs mainly in the zone within the wetting front, which accelerates the advance of the wetting front and decreases the slope stability. The coefficient of erosion flux rate, β_{er} of the erosion law, is the main factor that affects the internal erosion. The effect of erosion on the wetting front movement is more significant with large values of β_{er}. The effects of parameters i^* and α_{er} are less significant when compared with β_{er}. When the rainfall flux is equal or greater than the saturated coefficient of permeability, the influence of internal erosion on water infiltration and slope stability is significant. The effect of internal erosion can be neglected as long as the rainfall flux is less than the saturated coefficient of permeability. When the air-entry value of the soil is greater, the influence of internal erosion on infiltration and slope stability becomes less significant.

Keywords Rainfall · Infiltration · Slope stability · Internal erosion · Unsaturated soil · Flow

✉ Hua Zhang
cezhua@139.com

Lulu Zhang
lulu_zhang@sjtu.edu.cn

[1] State Key Laboratory of Ocean Engineering, Department of Civil Engineering, Shanghai Jiao Tong University, 800 Dongchuan Road, Shanghai, China

[2] Collaborative Innovation Center for Advanced Ship and Deep-Sea Exploration (CISSE), Shanghai 200240, China

[3] College of Civil Engineering and Architecture, Three Gorges University, Yichang Shi, China

[4] Key Laboratory of Geotechnical and Underground Engineering of Ministry of Education and Department of Geotechnical Engineering, Tongji University, Shanghai 200092, China

Introduction

Rainfall-induced landslides are common in many regions under tropical or subtropical climates (Lumb 1962; Brand 1984; Fourie 1996; Sidle and Ochiai 2006; Schuster and Highland 2007; Glade et al. 2006; Zhang et al. 2016a; Chen et al. 2017; Salciarini et al. 2017; Tang et al. 2017). The slope failures may occur on natural terrain slopes in a variety of materials including residual and colluvial soils (Dai et al. 2003; Crosta and Frattini 2003; Mondal and Mandal 2017; Vahedifard et al. 2017). The natural terrain slopes are usually composed of mixed coarse and fine particles due to deposition or weathering processes. In-situ full scale and laboratory reduced scale model tests showed that under rainfall infiltration, fine particles were transported from the upper part of the slope and slope surface to the toe due to internal erosion under the seepage flow (Crosta and di Prisco 1999; Hu et al. 2005; Jian et al. 2005).

Internal erosion has been extensively investigated in the stability of dams, levees and streambank (Fell et al. 2003; Wilson et al. 2007; Fox and Wilson 2010; Zhang and Chen 2006; Chang and Zhang 2010). For the problem of dam stability, internal erosion refers to the loss of soil particles within a dam or its foundation by seepage forces, and can be initiated

by concentrated leak erosion, backward erosion, contact erosion, or suffusion (Fell and Fry 2007; Xu and Zhang 2009; Peng and Zhang 2012; Zhang et al. 2016b). In this study, we focus on the internal erosion due to suffusion, which involves detachment and migration of fine particles within the matrix of coarse soil particles under seepage flow.

Geometric conditions (e.g., grain size distribution, pore size distribution, grain shape, and pore shape), hydraulic conditions (e.g., hydraulic gradient, seepage direction, pore fluid velocity, chemical property of the fluid), and mechanical conditions (e.g., compaction and stresses) affect the potential for internal erosion (Kenney et al. 1985; Wan and Fell 2008; Schuler 1995; Chang and Zhang 2011, 2013b). Tremendous research studies have been conducted to establish criteria of the potential of internal erosion based on laboratory tests, physical model tests and field observations (Istomina 1957; Kezdi 1969; Kenney and Lau 1985; Wan and Fell 2008; Fannin and Moffat 2006; Li and Fannin 2008; Indraratna et al. 2011; Sato and Kuwano 2015; Chang and Zhang 2011, 2013a). Substantial efforts have also been made to model particle transport and internal erosion problems such as piping (Fujisawa et al. 2010), streambank or riverbank stability (Wilson et al. 2007; Darby et al. 2007), ground subsidence (Sterpi 2003; Cividini et al. 2009) and sand production from oil wells (Papamichos and Vardoulakis 2005) through analytical or numerical methods.

The previous studies focus mostly on fully saturated porous media. Limited studies have been conducted to investigate the influences of internal erosion on unsaturated soil slopes, especially under the condition of rainfall infiltration along the slope surface. In the problem of slope stability under rainfall infiltration, the soils are unsaturated above the ground water level (Bass et al. 2017). The seepage in the vadose zone is important for soil shear strength and global slope stability (Ciervo et al. 2015; Giuseppe et al. 2016). When transport of fine particles occurs in a slope, the porosity and permeability may change due to variation of pore space and grain size distribution. This may further lead to variation of water flow or movement of a wetting front and affect the global stability during infiltration.

The objective of this study is to develop a model for coupled seepage and internal erosion in unsaturated soil slopes. The variation of porosity and grain size distribution due to particle transport is considered. A parametric study is conducted for a hypothetical slope to investigate the effect of internal erosion on water infiltration and slope stability.

Coupled model of unsaturated flow and internal erosion

Governing equations of flow and erosion

The soil is regarded as a mixture of solid and liquid which consists of soil skeleton phase, a water phase and a phase of liquefied particles, which are fine particles scoured by internal erosion from the soil skeleton and can move freely with water. The liquefied fine particles satisfy the mass conservation equation (Cividini and Gioda 2004):

$$\frac{\partial \rho_{tr}}{\partial t} + div(\rho_{tr} v_i) = q_{er} - q_{dp} \tag{1}$$

where ρ_{tr} is the density of liquefied fine particles; v_i is fluid velocity in the i direction; q_{er} is the volume flux of fine particles eroded from the soil skeleton; and q_{dp} is the volume flux of fine particles deposited on the soil skeleton.

The density of fine soil particles in the soil skeleton, ρ_f, is the difference between the initial density of a fine particle ρ_{f0} before the internal erosion starts and the density of liquefied fine particles ρ_{tr}:

$$\rho_f = \rho_{f0} - \rho_{tr} \tag{2}$$

Therefore, the governing equation for the fine particles in two dimensions can be expressed as:

$$\frac{\partial \rho_f}{\partial t} + \frac{\partial}{\partial x}\left(\rho_f v_x\right) + \frac{\partial}{\partial y}\left(\rho_f v_y\right) = -q_{er} + q_{dp} \tag{3}$$

The mass conservation of the soil skeleton phase can be expressed in a similar form as follows (Papamichos and Vardoulakis 2005):

$$\frac{\partial \rho_{sk}}{\partial t} + div\left(\rho_{sk} v_i^{sk}\right) = q_{dp} - q_{er} \tag{4}$$

where ρ_{sk} is the density of the soil skeleton and v_i^{sk} is the velocity of the soil skeleton. The density of soil skeleton ρ_{sk} is equal to $(1\text{-}n)\rho_s$, where ρ_s is the density of soil particles and n is the porosity. The velocity of the soil skeleton phase can be assumed to be zero. Therefore, the governing equation of the soil skeleton can be expressed as follows:

$$\frac{\partial n}{\partial t} = \frac{q_{er} - q_{dp}}{\rho_s} \tag{5}$$

Based on the mass conservation and Darcy's law, the governing equation for two-dimensional water flow in an unsaturated soil can be written as (Fredlund and Rahardjo 1993):

$$\frac{\partial}{\partial x}\left(k_x(\psi)\frac{\partial H}{\partial x}\right) + \frac{\partial}{\partial y}\left(k_y(\psi)\frac{\partial H}{\partial y}\right) = \frac{\partial \theta_w(\psi)}{\partial t} \tag{6}$$

where k_x and k_y are the coefficients of permeability in x and y directions, respectively; θ_w is the volumetric water content of the unsaturated soil. For an unsaturated soil, the volumetric water content θ_w and coefficient of permeability k are both related with matric suction $\psi = u_a - u_w$, where u_a is the pore-air pressure and u_w is the pore-water pressure. The relation between volumetric water content θ_w and matric suction ψ is named as a Soil Water Characteristic Curve (SWCC). The

relation between the coefficient of permeability k and matric suction ψ is called a permeability function. In this study, the air phase in unsaturated soil is assumed to be continuous and connects with the atmosphere. Hence, the pore-air pressure u_a is assumed to be zero. The SWCC and permeability function are, hence, expressed as functions of pore-water pressure u_w. Equations (3), (5) and (6) govern the coupled infiltration and internal erosion problem. It should be noted that only the change of porosity of the soil skeleton is considered in this study. The effects of deformation and stress changes on internal erosion should be conducted in a further study.

Constitutive laws for internal erosion

The constitutive law of internal erosion describes the process in which the water phase transforms the fine particles into a liquefied particle phase by erosion. Various erosion laws have been proposed in the literature. Most of these laws are empirical relations which relate the erosion rate to the flow characteristics (i.e., velocity, hydraulic gradient), porosity, density of particles, and empirical erosion coefficients (Partheniades 1965; Vardoulakis et al. 1996; Papamichos and Vardoulakis 2005; Govindaraju et al. 1995; Hanson and Simon 2001; Sterpi 2003; Seghir et al. 2014; Chetti et al. 2016).

In this study, the erosion law modified from Cividini and Gioda (2004) is used:

$$q_{er} = \beta_{er}|v|\left(\rho_f - \rho_{f\infty}\right) \tag{7}$$

where β_{er} is the coefficient of the erosion rate; $|v|$ is the magnitude of flow velocity; ρ_f is the density of the fine particles in the soil; and $\rho_{f\infty}$ is the long-term density of fine particles which can be expressed as:

$$\rho_{f\infty} = \begin{cases} \rho_{f0} - \left(\rho_{f0} - \rho_f^*\right) i/i^* & 0 \le i \le i^* \\ \rho_f^* - \alpha_{er}\log\left(i/i^*\right) & i > i^* \end{cases} \tag{8}$$

where i^* is the hydraulic gradient when erosion starts; ρ^*_f is the density of fine particles corresponding to i^*; and α_{er} is a parameter of the erosion law. This erosion law implies that if sufficient time is allowed, the erosion process will remove the fine particles until the long-term density $\rho_{f\infty}$ is reached ($\rho_{f0} \rightarrow \rho_{f\infty}$).

In the original model proposed by Cividini and Gioda (2004), the flow velocity is used in quantifying $\rho_{f\infty}$. Based on previous studies, the hydraulic gradient is often used to describe the critical hydraulic conditions which govern the onset of internal erosion. Therefore, a critical hydraulic gradient i^* instead of a critical velocity v^* is used to describe the initiation of erosion in this study. Figure 1 shows the long-term density of fine particles $\rho_{f\infty}$ varies with the hydraulic gradient according to Eq. (8). The curve is based on fitting

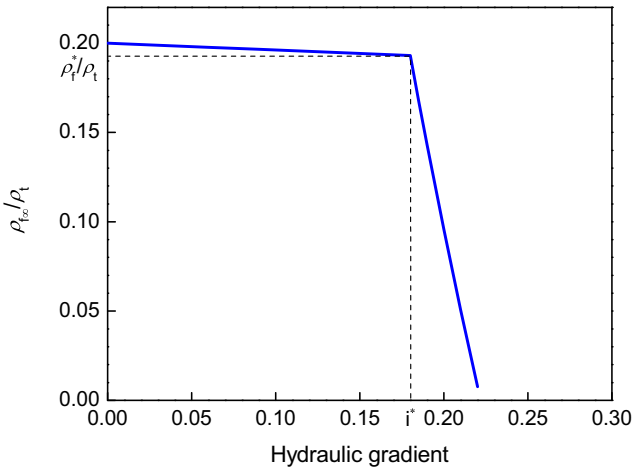

Fig. 1 Relation between the long-term density of fine particles $\rho_{f\infty}$ and hydraulic gradient i

the laboratory test results of silty sands (Sterpi 2003; Cividini and Gioda 2004). In the experimental work by Sterpi (2003), the soil from the urban area of Milano (Italy) was used. The in situ soil consisted of well graded sand and gravel. For the laboratory tests, only the material passing through an ASTM 10 sieve (D = 2 mm) was considered and the soil particles passing through the standard ASTM 200 sieve (D = 0.074 mm), were referred to as fine particles. A standard ASTM 200 sieve was placed in the outflow and used to separate the fine particles from coarser grains possibly eroded from the soil primary fabric. The amount of coarser grains collected in the sieve was found to be negligible in all the series of experiments, even for the highest applied gradients. The initial fine particle content is 20% of ρ_t, where ρ_t is the total density of the soil. ρ^*_f is assumed to be 96.5% of ρ_{f0}, i.e., 19.3% of ρ_t. The critical hydraulic gradient i^* is 0.18 and α_{er} is 4.76. As shown in the graph, $\rho_{f\infty}$ is reduced drastically if the hydraulic gradient is greater than i^*.

Hydraulic functions of unsaturated soil

In this study, the van Genuchten-Mualem (van Genuchten 1980; Mualem 1976) model, is adopted for the SWCC and the permeability function of unsaturated soil. The van Genuchten-Mualem SWCC model is expressed as:

$$\theta_w = \begin{cases} \theta_r + \dfrac{\theta_s - \theta_r}{\left[1 + \left[\alpha_w(-u_w)\right]^{n_w}\right]^{m_w}} & u_w < 0 \\ \theta_s & u_w \ge 0 \end{cases} \tag{9}$$

where θ_s is the saturated volumetric water content; θ_r is the residual volumetric water content; α_w is a curve fitting parameter inversely related to the air-entry value; n_w is a curve-fitting parameter related to the pore size distribution; and m_w is a parameter with $m_w = 1 - 1/n_w$ (Mualem 1976).

The coefficient of permeability function is expressed as (van Genuchten 1980; Mualem 1976):

$$k = \begin{cases} k_s \dfrac{\left\{1-(-\alpha_w u_w)^{n_w-1}\left[1+(-\alpha_w u_w)^{n_w}\right]^{-m_w}\right\}^2}{\left[1+(-\alpha_w u_w)^{n_w}\right]^{m_w/2}} & u_w < 0 \\ k_s & u_w \geq 0 \end{cases} \quad (10)$$

where k_s is the saturated coefficient of permeability.

To consider the effect of internal erosion on the hydraulic properties, the saturated coefficient of permeability is defined as a function of porosity based on the Kozeny-Carman equation (Kozeny 1927; Carman 1937, 1956):

$$k_s = \frac{n^3}{(1-n)^2} \times \frac{(1-n_0)^2}{n_0^3} k_{s0} \quad (11)$$

where n_0 is the initial porosity before internal erosion starts; k_{s0} is the initial saturated coefficient of permeability corresponding to n_0.

Finite element model and soil parameters

Figure 2 shows the finite element model of a hypothetical slope with a slope angle β of 35°. The slope is composed of residual soils. The thickness of the soil layer is 6 m. The finite element model is composed of 1100 quadrilateral elements.

For the governing equation of water flow in Eq. (6), the initial ground water table is along BC. Under the rainfall infiltration, the water levels along the boundaries AB, BC and CD are fixed as the initial ground water table. The infiltration flux along the slope surface AD is defined as (Chui and Freyberg 2009):

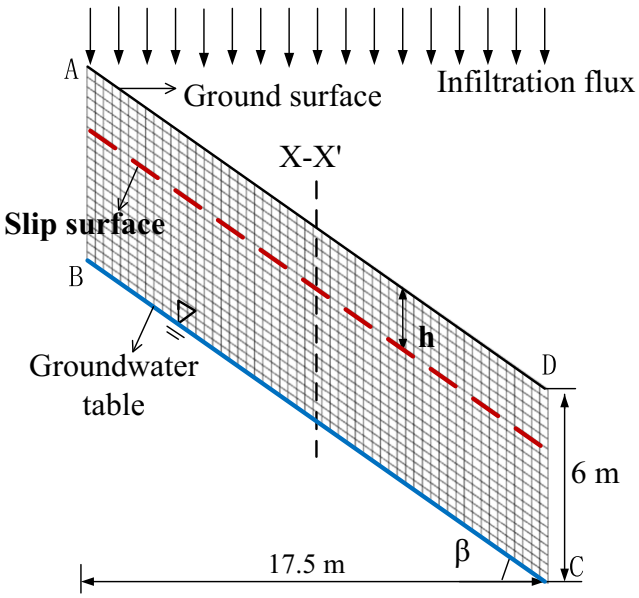

Fig. 2 Finite element model of the illustrative example

$$flux = m_N(u_w)q + m_b(u_w)R_b(-u_w/\gamma_w) \quad (12)$$

where *flux* = infiltration flux; m_N, m_b = complementary smoothing functions (Fig. 3); R_b = external resistance; and q = rain intensity. This infiltration flux boundary condition implies that when the pore water pressure at the slope surface AD is negative, the infiltration flux is equal to rainfall intensity q. When the pore water pressure at the slope surface AD is positive, the infiltration flux is negative to guarantee no ponding on the slope surface.

The governing equation of ρ_f, Eq. (3) is a first-order partial differential equation. The mass transport is due to convection. The initial density of fine particles is set to a given value ρ_{f0}. The velocity of a liquefied particle is zero along the boundaries AB, BC and AD. The density of fine particles at the lower vertical boundary CD is set to be 50% ρ_{f0} in order to prevent accumulation of particles at the lower boundary. The governing equation of porosity n, Eq. (5), is an ordinary differential equation. The variation of porosity only depends on the internal erosion. The initial condition is a homogenous porosity field and no boundary conditions are necessary.

The unsaturated hydraulic parameters are assumed to represent silty sands (Santoso et al. 2011). The SWCC and permeability function of the soil are shown in Fig. 4. The saturated permeability of the soil is assumed to be 2×10^{-4} m/s. The erosion parameters are assumed based on the laboratory test results of silty sands in Sterpi (2003). The initial fine particle content is 20% of ρ_t, where ρ_t is total density of the soil. ρ^*_f is assumed to be 96.5% of ρ_{f0}, i.e., 19.3% of ρ_t. The other parameters are obtained by fitting laboratory test curves (Cividini and Gioda 2004). The critical hydraulic gradient i^* is 0.18. The α_{er} and β_{er} are 4.76 and 1.95×10^{-3}, respectively. Table 1 summarizes the input parameters in the numerical model.

Numerical simulation and slope stability analysis

A finite element model based on the coupled governing equations [Eqs. (3), (5), and (6)] is developed in the multiphysics modeling finite element program, COMSOL (COMSOL 2010). First, the partial differential equations (PDEs) [Eqs. (3), (5), and (6)] are formulated in the PDE coefficient form module using the graphical user interface (GUI). The boundary conditions and initial conditions are also formulated in PDE coefficient forms. Then, the Galerkin method is used to discretize the partial differential equations. A nonlinear differential algebraic equation solver IDA

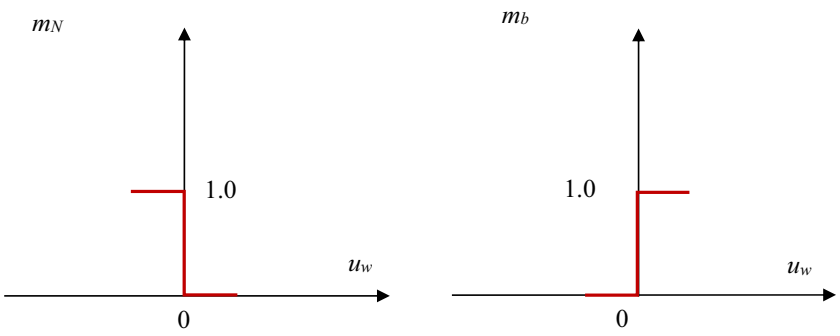

Fig. 3 Function m_N and m_b

that was created by the Lawrence Livermore National Laboratory (Hindmarsh et al. 2005) is used as a time integrator for the differential algebraic system, in which the backward differentiation formulas (BDF) are used to discretize the time derivative terms. The solver name IDA stands for Implicit Differential-Algebraic. As the time stepping scheme is implicit, the damped Newton method (Deuflhard 1974) is then used to solve the resulting nonlinear equations. Within each step of the Newton iteration, the most recently updated nodal values of the dependent variables are used to compute nonlinear coefficients. The nonlinear iteration at each time step is continued until the numerical solutions satisfy prescribed convergence criteria for pressure head and displacement. In this study, the absolute tolerance is set to be 0.001, and the relative tolerance is set to be 0.01.

Since slope failures induced by rainfall infiltration are usually shallow, infinite slope stability analysis may be appropriate for evaluating the stability of soil slopes under rainfall. The safety factor for the slip surface at depth h (Figure 2) is (Iverson 2000; Cho and Lee 2002):

$$F_s = \frac{c'}{\gamma_t h \sin\beta \cos\beta} + \frac{\tan\phi'}{\tan\beta} - \frac{h_w \gamma_w \tan\phi^b}{\gamma_t h \tan\beta} \tag{13}$$

where β is the slope angle; γ_t is the total unit weight of the soil; c' is the effective cohesion; ϕ' is the effective friction angle; h is the depth of the slip surface (Fig. 2); h_w is the pore water pressure head; γ_w is the unit weight of water; and ϕ^b is the angle indicating the rate of increase in shear strength related to matrix suction. In the example shown in Fig. 2, c' is assumed to be 2 kPa. The value of ϕ^b depends on the matric suction and is generally around 1/3 to 2/3 of ϕ'; here, ϕ' and ϕ^b are assumed to be 34° and 25°, respectively. The distribution of the pore water pressure head from the numerical simulation is used in calculating the safety factor.

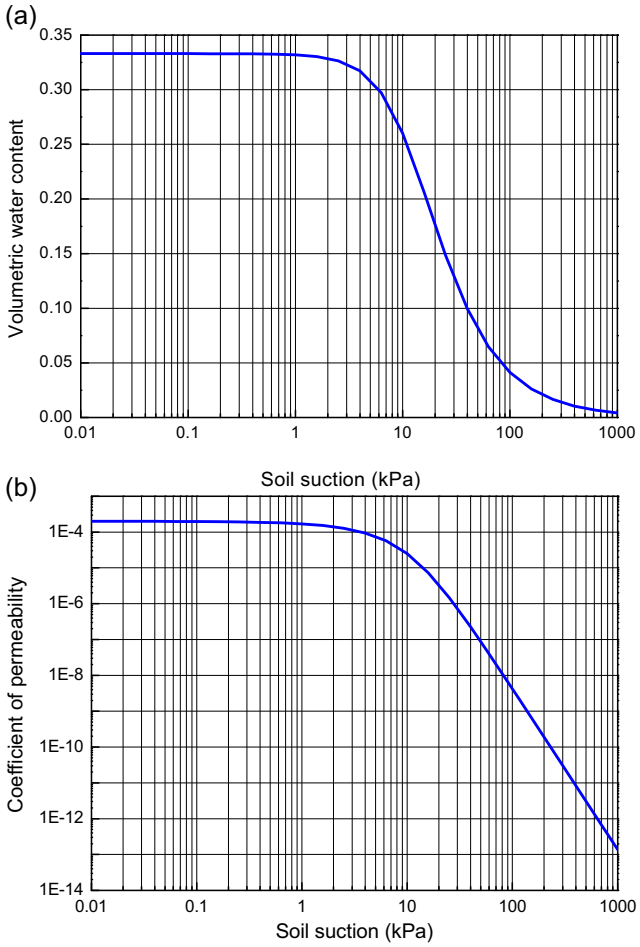

Fig. 4 The SWCC and permeability function of the residual soil

Table 1 List of parameters in the numerical model

Parameters	Value	Parameters	Value
ρ_{f0}/ρ_t	0.2	θ_r	0
ρ^*_f/ρ_{f0}	0.965	θ_s	0.333
ρ_t (g/cm^3)	2.24	n_0	0.333
$i^*{}_s$	0.18	α_w (kPa^{-1})	0.08
α_{er}	4.76	n_w	2
β_{er}	1.95×10^{-3}	β (°)	35
R_b	10^3	ϕ'(°)	34
k_{s0} (m/s)	2×10^{-4}	c' (kPa)	2
q (m/s)	2×10^{-4}	ϕ^b (°)	25

Analysis results and discussion

Effects of internal erosion on infiltration and slope stability

The slope is subject to a rainfall with a constant flux of $q = 2\times10^{-4}$ m/s. To analyze the influence of internal erosion on the slope stability, the results of the coupled analysis of flow and internal erosion are compared with those without considering internal erosion.

As shown in Fig. 5, the depth of the wetting front is deeper when considering internal erosion. After 68 min of rainfall, the unsaturated zone is fully saturated if internal erosion is considered. However, there is still a 2.0 m thick soil that is unsaturated if the internal erosion is neglected. The differences between the coupled and uncoupled analysis become more significant as the infiltration progresses.

Figure 6 shows the variation of fine particle content and porosity along the cross-section X–X′ in the middle part of the slope. It can be seen that internal erosion occurs mainly at the shallow depths of the slope. The variation of the fine content and porosity in the shallow soil develop almost simultaneously with the advance of the wetting front. The fine particles around the groundwater table are also eroded slightly. This is mainly because, when the soil is almost saturated, the flow velocity is large enough to transport the fine particles based on the erosion law in Eq. (7).

Figure 7 presents the profiles of the hydraulic gradient at different times of rainfall. The hydraulic gradients are all greater than 0.57 in the unsaturated zone. Extremely large hydraulic gradients of more than 8 appear near the wetting fronts. As the unsaturated zone is fully saturated (t = 68 min), the gradient is reduced significantly but is still greater than 1.0.

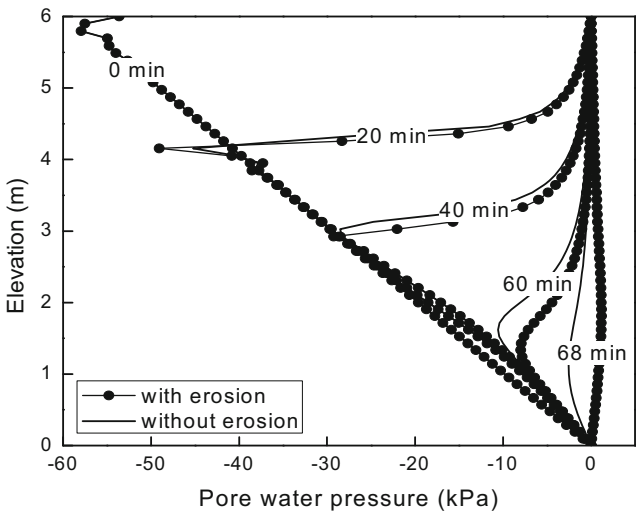

Fig. 5 Variation of pore-water pressure profile along cross-section X–X′ in Fig. 2 ($k_{s0} = 2 \times 10^{-4}$ m/s, $\beta_{er} = 1.95 \times 10^{-3}$)

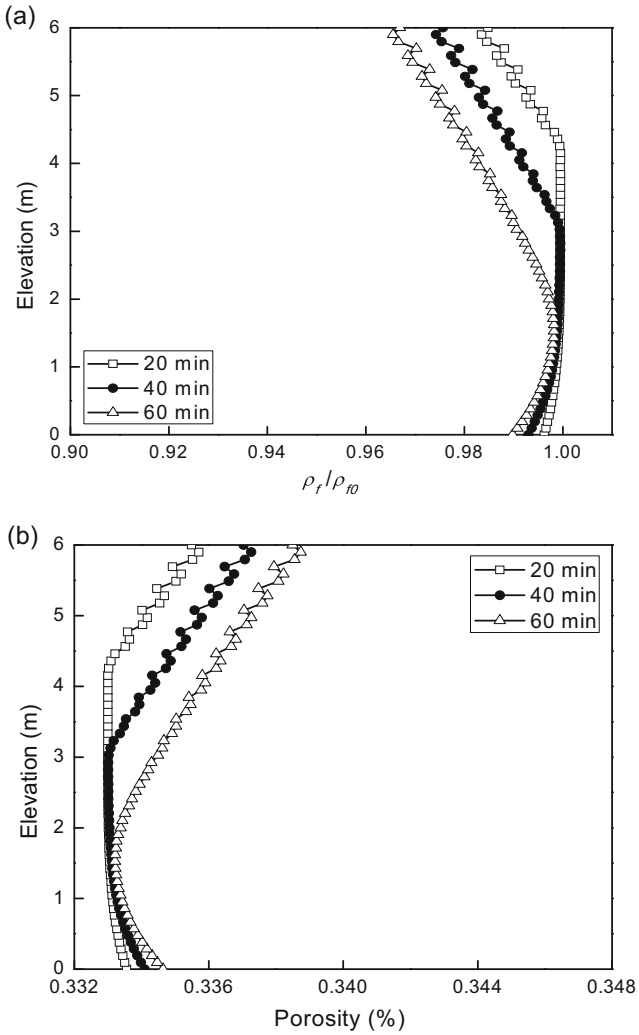

Fig. 6 Variation of (**a**) fine particle content ρ_f/ρ_{f0} and (**b**) porosity with time along cross-section X–X′ ($k_{s0} = 2 \times 10^{-4}$ m/s, $\beta_{er} = 1.95 \times 10^{-3}$)

Figure 8 shows the safety factor of the slope along various depths of the slip surface. The soil slope reaches an unstable state more rapidly when considering the internal erosion. After 68 min of infiltration, the critical slip surface is around 3.0 m, and the factor of safety of the slope is less than 1.0. However, the factor of safety of the slope without internal erosion is still greater than 1.0. This result implies that internal erosion may lead a more abrupt landslide.

Effects of erosion parameters

As shown in Eqs. (7) and (8), the four parameters, β_{er}, i^*, ρ^*_f, and α_{er} can influence the development of erosion. The ρ^*_f represents the fine particle density corresponding to the initiation of erosion and is generally very close to the initial value of ρ_f. Hence, in this example, ρ^*_f is assumed to be constant.

Terzaghi (1939) defined a critical hydraulic gradient for the upward flow condition in which the soil is unstable when the effective stress becomes zero. The critical hydraulic gradient

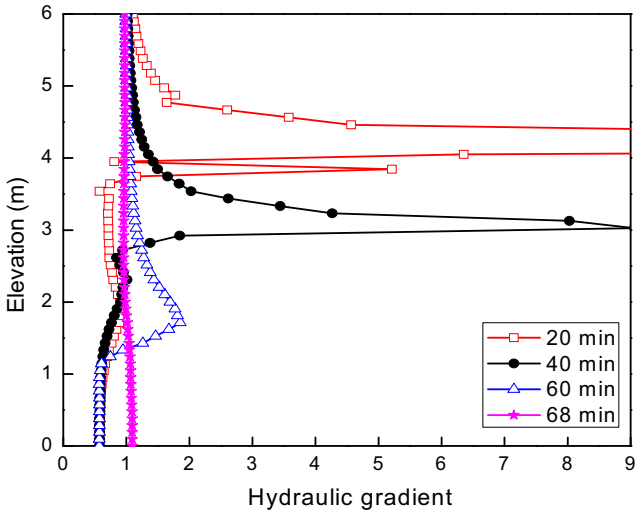

Fig. 7 Hydraulic gradients along cross-section X–X′ ($k_{s0} = 2 \times 10^{-4}$ m/s, $\beta_{er} = 1.95 \times 10^{-3}$)

is typically about 1.0. Skempton and Brogan (1994) showed that the critical hydraulic gradient for internally unstable sandy gravels is only about one fifth to one third (i.e., 0.2 to 0.34) of the theoretical value given by Terzaghi (1939). Wan and Fell (2008) investigated silt-sand-gravel or clay-silt-sand-gravel soils and found loose higher porosity soils began to erode at gradients less than 0.3. The critical hydraulic gradient in a horizontal flow condition for very unstable gravel soils could be even smaller (i.e., 0.16 as reported in Adel et al. 1988, samples are of large dimensions and in a loose state of packing). The explanation for the small critical gradients is that a major part of the overburden load is carried by the skeleton of gravel, leaving the fine particles under relatively small pressures (Skempton and Brogan 1994). These previous studies confirm that the measured value of 0.18 for i^* in Sterpi (2003) is reasonable for unstable soils.

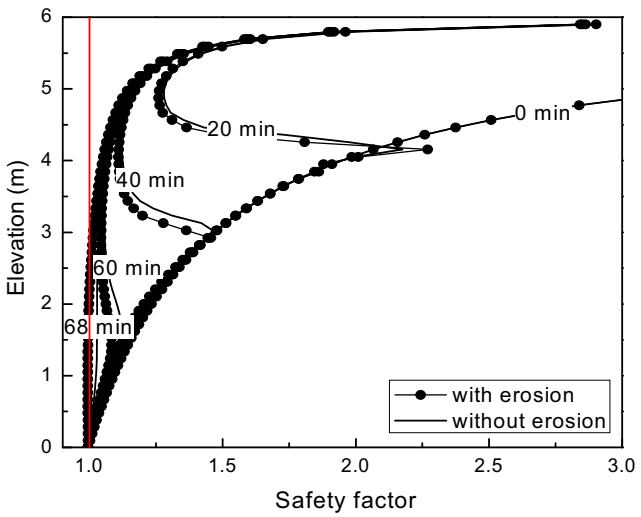

Fig. 8 Profile of safety factor at different times ($k_{s0} = 2 \times 10^{-4}$ m/s, $\beta_{er} = 1.95 \times 10^{-3}$)

Very limited studies have laboratory measurements of the amount of removed particles lost with time (Chang and Zhang 2013a). Therefore, the possible range of the fitting erosion parameters β_{er} and α_{er} can hardly be obtained. The hole erosion test (HET) and the slot erosion test (SET) have been developed to study rates of erosion and the critical hydraulic shear stress to initiate piping erosion. An approximately linear relation between the rate of erosion and the applied hydraulic shear stress has been found based on the laboratory test results (Hanson and Simon 2001; Briaud et al. 2001; Wan and Fell 2004; Bonelli and Brivois 2008; Chang et al. 2011). The empirical relation is expressed as:

$$\dot{\varepsilon} = C_e(\tau - \tau_c) \tag{14}$$

where $\dot{\varepsilon}$ is the erosion rate of the soil per unit surface area of the slot/hole (kg/s/m^2); C_e is the coefficient of soil erosion; τ_c is the critical shear stress of soil at initiation of erosion (N/m^2); and τ is the hydraulic shear stress along the slot/hole (N/m^2) which can be obtained based on the hydraulic gradient across the soil sample. For example, in the HET, the hydraulic shear stress along the pre-formed hole is:

$$\tau_{HET} = \gamma_w i_{HET} \frac{\phi_{HET}}{4} \tag{15}$$

where τ_{HET} is the hydraulic shear stress on the surface of the pre-formed hole; i_{HET} is the hydraulic gradient across the soil sample; and ϕ_{HET} is the diameter of the hole, assumed to remain circular.

According to Wan and Fell (2004), the coefficient of soil erosion C_e obtained for the various HETs or SETs are on the order of 10^{-1} to 10^{-6}. Equation (7) is similar to Eq. (14) as both equations are approximately linear. Hence, coefficient β_{er} is similar to the coefficient of soil erosion C_e and can vary within a large range depending on the basic soil properties such as grain size distribution, relative density, etc. In this example, the effects of the erosion parameters β_{er} and α_{er} on erosion and infiltration are investigated by parametric studies.

Figure 9 shows the variation of fine content and pore-water pressure profiles when β_{er} is increased to 0.005 and 0.01. Comparing Fig. 9 to Fig. 5, the dissipation of matric suction is much faster, and the difference between the coupled and uncoupled analysis is greater when β_{er} is increased from 1.95×10^{-3} to 0.01. The effect of erosion on the wetting front movement is more significant with a larger value of β_{er}. The main reason is that when β_{er} is increased, the erosion rate increases (Eq. 7). Consequently, the porosity is increased more significantly and the hydraulic conductivity in the unsaturated zone is significantly increased.

Figure 10 shows the pore water pressure profiles in the unsaturated zone with different values of i^*. When the critical gradient of initiation is increased to 1.0, the effect of the

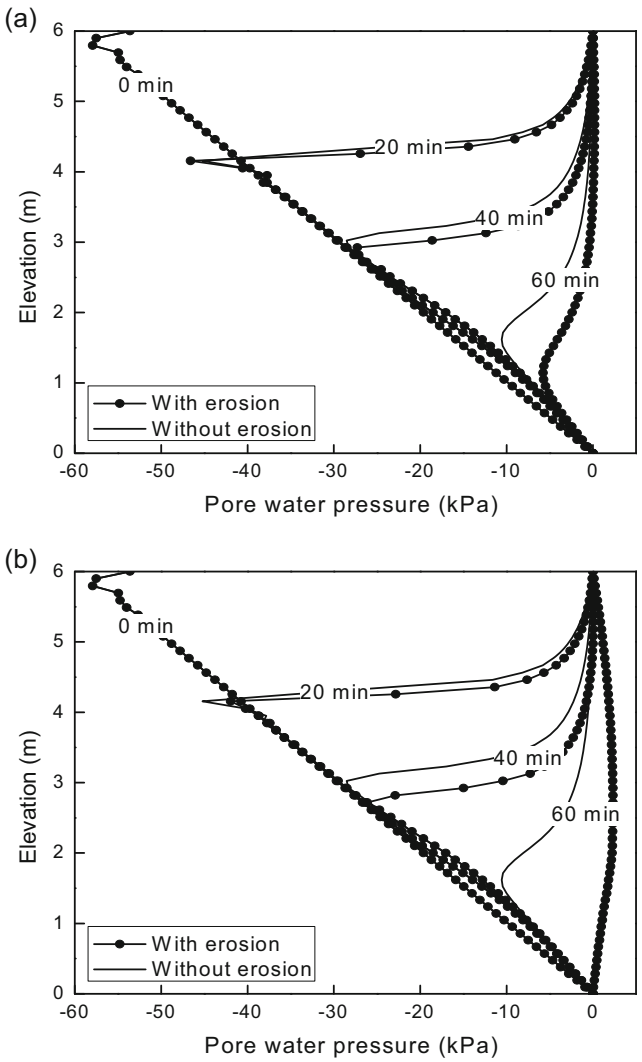

Fig. 9 Variation of pore-water pressure profiles along cross-section X–X′ (**a**) β_{er} = 0.005 and (**b**) β_{er} = 0.01

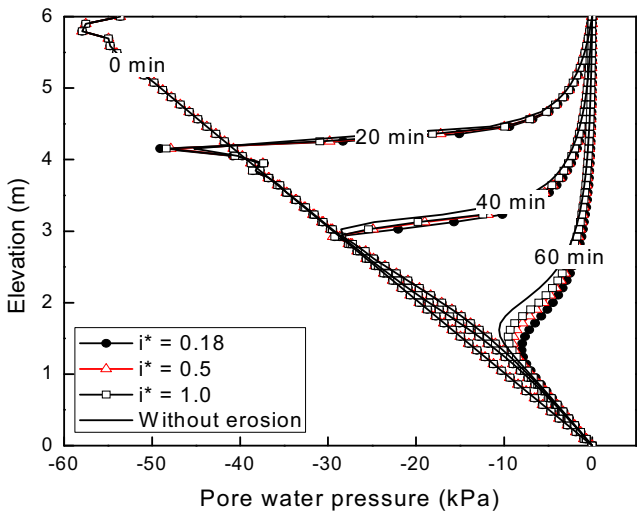

Fig. 10 Comparison of pore-water pressure profiles with different values of i^*

internal erosion on the advance of the wetting front is reduced. The result of i^* of 0.5 is not much different from that of 1.0.

As shown in Eq. (8), the erosion parameter α_{er} influences the long term density of fines $\rho_{f\infty}$. Figure 11 shows that after the initiation of erosion, the slope of the curve for $\rho_{f\infty}$ is gentler if α_{er} is smaller. Hence, the long-term density of fine particles, which can be maintained in the slope, is greater even if the flow field does not change. Figure 12 compares the pore water pressure profiles for different values of α_{er}. As shown in the graph, when α_{er} is 0.5, the effect of erosion on pore water pressure distributions is reduced.

Comparing Figs. 9, 10, and 12, β_{er} is the main factor that affects the internal erosion in a slope. The effect of erosion on the wetting front movement is more significant with large values of β_{er}. The effects of i^* and α_{er} are less significant when compared with β_{er}.

Effect of soil hydraulic parameters

To investigate the effects of soil hydraulic properties on the coupled analysis, the saturated coefficient of permeability and the air-entry value parameter of the SWCC model, which have been identified as the two most important hydraulic parameters (Zhang et al. 2016a), are selected for a parametric study.

Three different values of the initial saturated coefficient of permeability k_{s0}, 5×10^{-5}, 2×10^{-4} and 8×10^{-4} m/s are adopted in the parametric study. The other parameters are the same as those in Table 1. Figure 13 shows the pore water pressure profiles with different values of k_{s0}. For a soil slope with k_{s0} equal to 5×10^{-5} m/s (Fig. 13a), the internal erosion has little effect on the pore water pressure profile before 80 min of rainfall. After 80 min, the advance of the wetting front becomes faster and the effect of internal erosion is more obvious. However, the effect of internal erosion is still less significant than the case with k_{s0} equal to 2×10^{-4} m/s. When k_{s0} is increased to 8×10^{-4} m/s, the rainfall intensity is smaller than the saturated permeability, and; hence, the

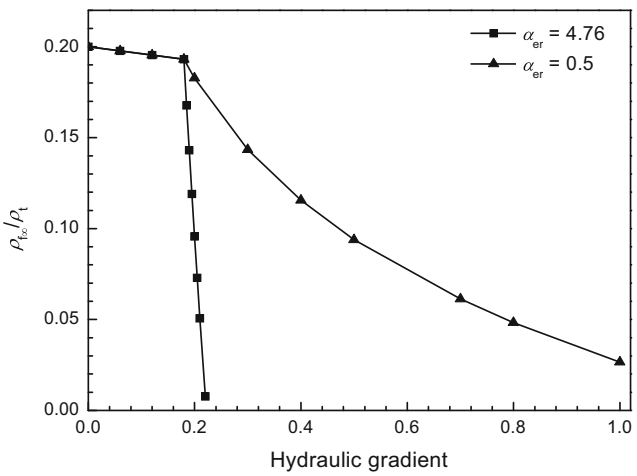

Fig. 11 Effect of the parameter α_{er} on the erosion function $\rho_{f\infty}$

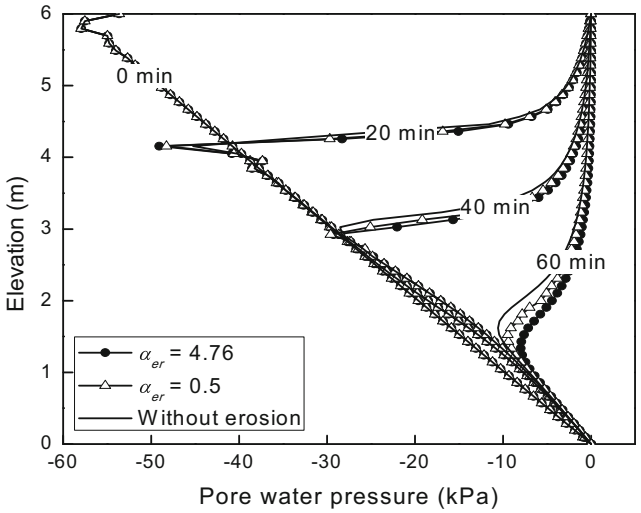

Fig. 12 Comparison of pore-water pressure profiles for different values of α_{er}

matric suction can be maintained even after a long duration of rainfall (Zhang et al. 2004). The internal erosion increases the depth of the wetting front only slightly for this case. Comparing the three graphs in Fig. 13, the influence of internal erosion on water infiltration is significant only when the rainfall flux is equal or greater than the saturated coefficient of permeability ($q/k_{s0} \geq 1$).

Figure 14 presents the comparison of the pore water pressure profiles with different values of k_{s0} for a more instable soil (β_{er} = 0.01). It shows that the internal erosion is more significant for the two cases with $q/k_{s0} \geq 1$. There are some effects of erosion for the case with k_{s0} equal to 8×10^{-4} m/s ($q/k_{s0} < 1$). However, this minor effect of internal erosion can be considered as negligible even for the more instable soil.

The air-entry value (AEV) of a soil is the matric suction where air starts to enter the largest pores in the soil. In the van Genuchten-Mualem SWCC model, the curve-fitting parameter α_w is inversely related to the air-entry value. In this study, the responses of soil slopes with different values of α_w, 0.04, 0.08 and 0.12, which correspond to AEV values of 25,12.5 and 8.33 kPa, respectively, are compared. The soil water characteristic curves and unsaturated permeability functions of the unsaturated soils with different values of α_w are presented in Fig. 15. Figure 16 shows the pore water pressure profiles in the soil slopes with different values of α_w. To demonstrate the effect of the parameter α_w more clearly, β_{er} is taken as 0.01. As shown in the graphs, with a smaller α_w (a larger AEV), the wetting process is faster in the unsaturated zone. When α_w is equal to 0.04, the effect of internal erosion on infiltration is initially very limited and becomes observable only when the unsaturated zone is almost fully saturated. When α_w is 0.12, the influence of internal erosion on infiltration is observable after the depth of wetting front is less than 2 m. As a coarser soil is usually related with a smaller AEV and, hence, a larger

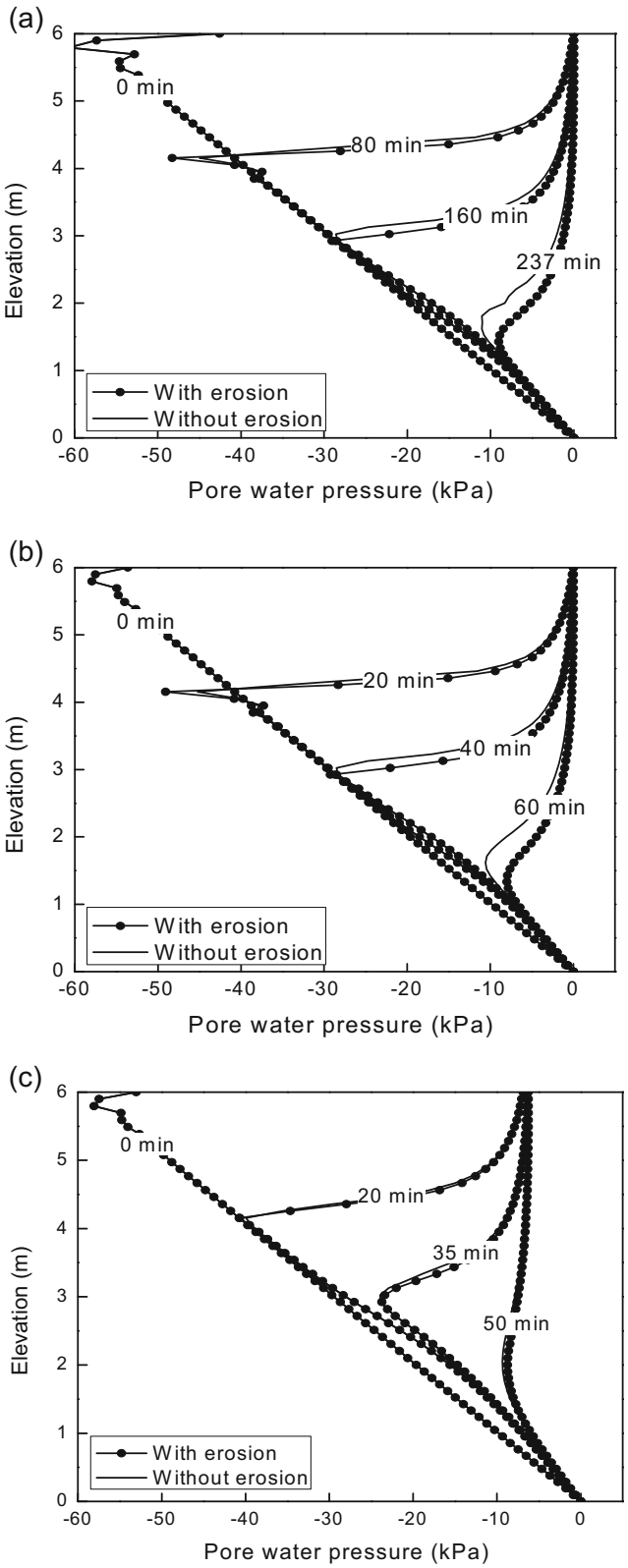

Fig. 13 Variation of the pore-water pressure profile along cross-section X–X′ with different values of k_{s0}: **a** 5×10^{-5} m/s, **b** 2×10^{-4} m/s, and **c** 8×10^{-4} m/s ($\beta_{er} = 1.95 \times 10^{-3}$)

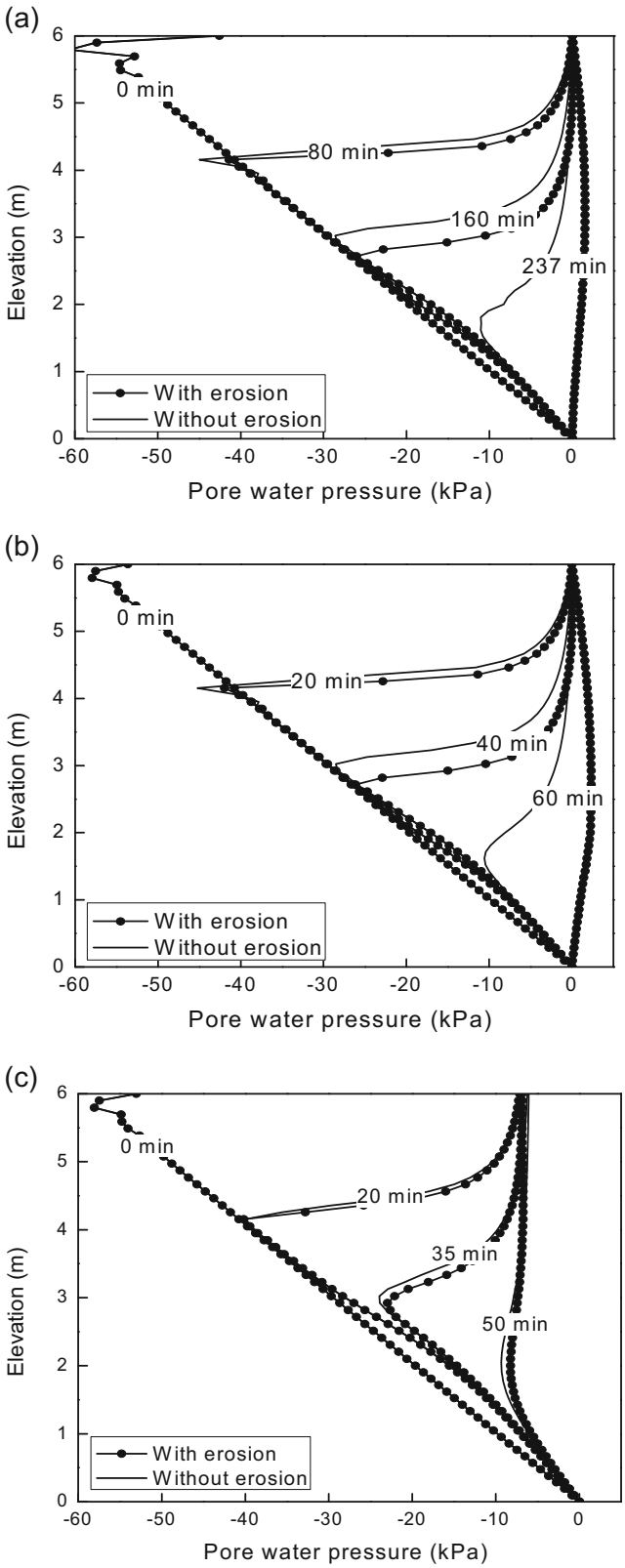

Fig. 14 Variation of the pore-water pressure profile along cross-section X–X′ with different values of k_{s0}: **a** 5×10^{-5} m/s, **b** 2×10^{-4} m/s, and **c** 8×10^{-4} m/s ($\beta_{er} = 0.01$)

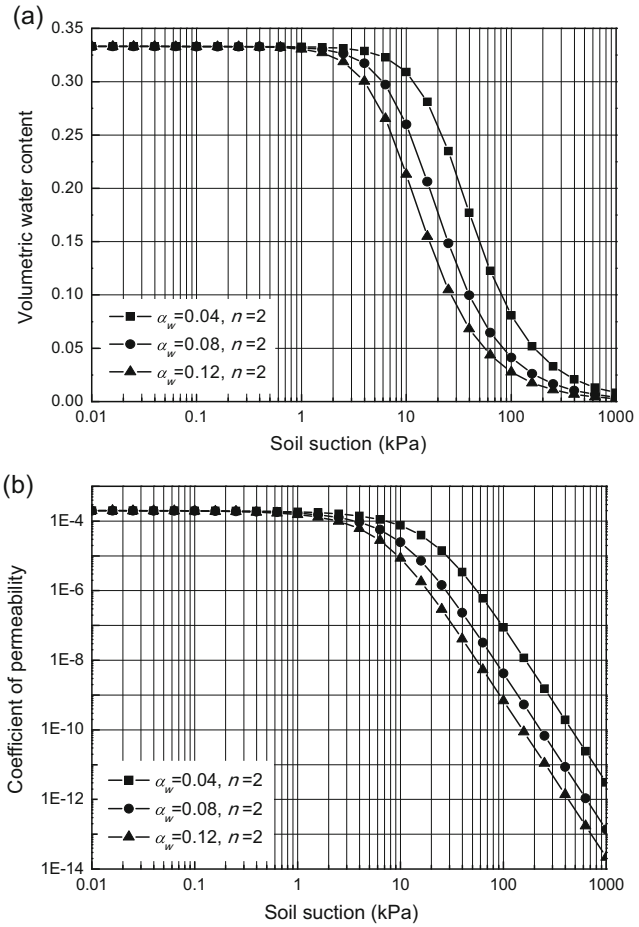

Fig. 15 Soil water characteristic curves and unsaturated permeability functions of the unsaturated soils with various values of α_w

α_w, these results imply that the internal erosion may be more influential in a coarse soil slope.

Conclusions

In this study, a coupled model of seepage and internal erosion in unsaturated soil is established to investigate the effects of internal erosion on water infiltration and slope stability. The major conclusions are as follows:

1. The soil porosity increases with the advance of the water front and the procession of internal erosion. The advance of the wetting front in the slope is more rapid and the slope reaches an unstable state more quickly due to internal erosion.
2. The parameter β_{er} of the erosion law is the major factor that affects the internal erosion in a slope. The effect of erosion on the wetting front movement is more significant with large values of β_{er}. The effects of parameters i^* and α_{er} are less significant when compared with β_{er}.

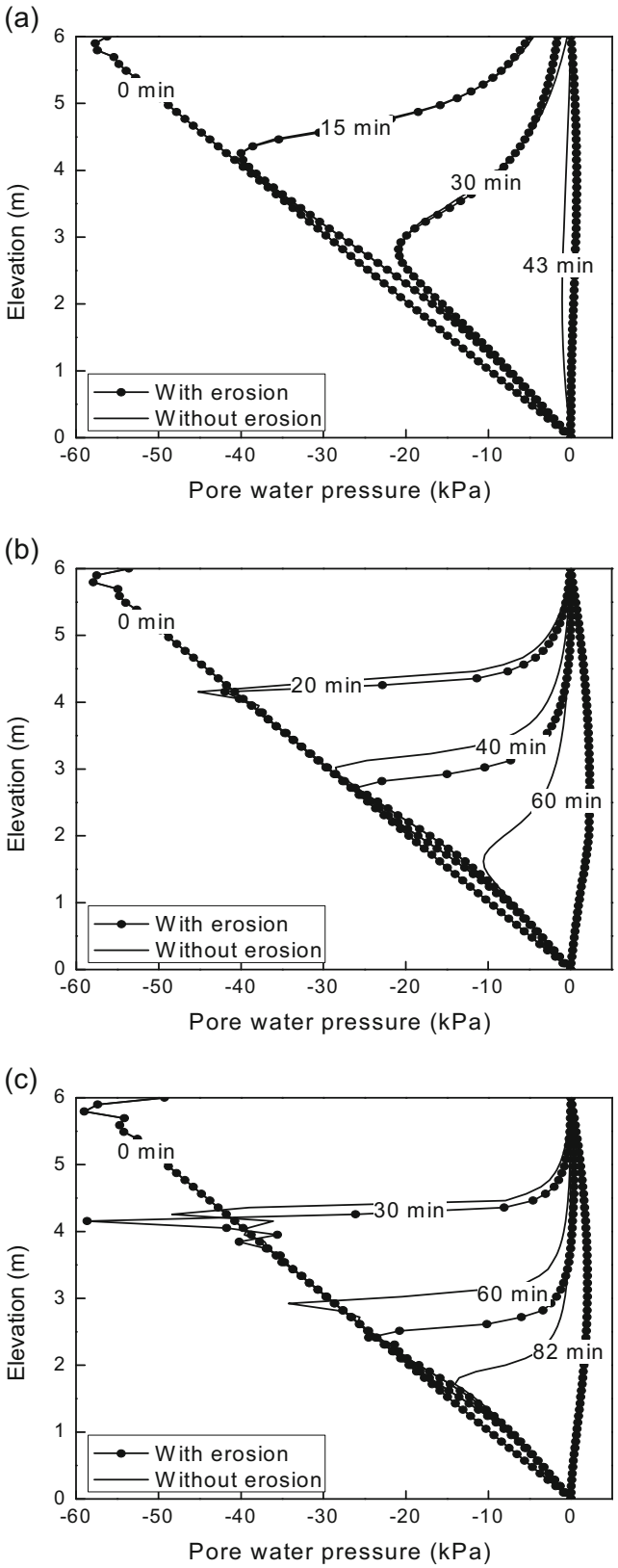

Fig. 16 Pore-water pressure profiles with different values of α_w: **a** 0.04, **b** 0.08 **c** 0.12 (β_{er} = 0.01)

3. When the rainfall flux is equal or greater than the saturated coefficient of permeability ($q/k_{s0} \geq 1$), the influence of internal erosion on water infiltration and slope stability is more significant. The effect of internal erosion can be neglected as long as the rainfall flux is less than the saturated coefficient of permeability.
4. When the soil is coarser and the air-entry value of the soil is smaller, the influence of internal erosion on infiltration becomes more significant.

In this study, the measurement or estimation of the erosion and hydraulic parameters, especially β_{er}, k_{s0} and the air entry value parameter α_w, are essential when analyzing a slope problem in practice using the proposed model. It is suggested the saturated permeability and the erosion parameters should be measured through laboratory column tests. The unsaturated hydraulic functions can be estimated through the grain size distribution or soil basic properties (Fredlund et al. 2002; Johari et al. 2006; Vereecken et al. 2010; Zhang and Chen 2005; Li et al. 2014).

The significance of the proposed method is that the method provides a practical and quantitative tool to evaluate the effects of internal erosion on rainfall-induced landslides. It should be noted the proposed coupled model of flow and internal erosion is based on the basic assumptions of unsaturated transient flow, e.g., Darcy's law, and the mass conservation of soil skeleton. The erosion law adopted is an empirical relation based on experimental results of a specific soil. The particle transport under the condition of non-Darcy's flow (Beven and Germann 1982; Chen et al. 2015) is not considered. The effect of particle deposition (Chen and Zhang 2015) and the deformation of the soil skeleton (Cho and Lee 2001; Alonso et al. 2003; Ye et al. 2005; Chen et al. 2009; Wu and Zhang 2009; Borja and White 2010; Cascini et al. 2010; Xiong et al. 2014) are not considered.

Acknowledgements The work in this paper was substantially supported by the National Basic Research Program of China (973 Program, Project No. 2014CB049100), and the Natural Science Foundation of China (Project No. 51422905, No. 51679135 and No. 41672276). The authors are grateful to the National Program for support of Top-notch Young Professionals. The constructive comments by Prof. Limin Zhang of the Hong Kong University of Science and Technology for preparing this paper are highly appreciated.

References

Adel HD, Bakker KJ, Breteler MK (1988) Internal stability of minestone. Proceedings of international symposium of modelling soil-water-structure interaction. Balkema, Rotterdam, pp 225–231

Alonso EE, Gens A, Delahaye CH (2003) Influence of rainfall on the deformation and stability of a slope in overconsolidated clays: a case study. Hydrogeol J 11(1):174–192

Bass B, Cardenas MB, Befus KM (2017) Seasonal shifts in soil moisture throughout a semiarid hillslope ecotone during drought: a geoelectrical view. Vadose Zone J 16(2). https://doi.org/10.2136/vzj2016.11.0108

Beven K, Germann P (1982) Macropores and water flow in soils. Water Resour Res 18(5):1311–1325

Bonelli S, Brivois O (2008) The scaling law in the hole erosion test with a constant pressure drop. Int J Numer Anal Methods 32(13):1573–1595

Borja RI, White JA (2010) Continuum deformation and stability analyses of a steep hillside slope under rainfall infiltration. Acta Geotech 5(1):1–14

Brand EW (1984) Landslides in south Asia: a state-of-art report. Proceedings of the 4th International Symposium on Landslides, Toronto, Canada, pp 17-59

Briaud JL, Ting FCK, Chen HC, Cao Y, Han SW, Kwak KW (2001) Erosion function apparatus for scour rate predictions. J Geotech Geoenviron Eng 127(2):105–113

Carman PC (1937) Fluid flow through granular beds. Trans Inst Chem Eng 15:150–156

Carman PC (1956) Flow of gases through porous media. Academic Press Inc, New York

Cascini L, Cuomo S, Pastor M, Sorbin G (2010) Modelling of rainfall-induced shallow landslides of the flow-type. J Geotech Geoenviron Eng 136(1):85–98

Chang DS, Zhang LM (2010) Simulation of the erosion process of landslide dams due to overtopping considering variations in soil erodibility along depth. Nat Hazards Earth Syst Sci 10(4):933–946

Chang DS, Zhang LM (2011) A stress-controlled erosion apparatus for studying internal erosion in soils. Geotech Test J 34(6):579–589

Chang DS, Zhang LM (2013a) Critical hydraulic gradients of internal erosion under complex stress states. J Geotech Geoenviron Eng 139(9):1454–1467

Chang DS, Zhang LM (2013b) Extended internal stability criteria for soils under seepage. Soils Found 53(4):569–583

Chang DS, Zhang LM, Xu Y, Huang RQ (2011) Field testing of erodibility of two landslide dams triggered by the 12 may Wenchuan earthquake. Landslides 8(3):321–332

Chen HX, Zhang LM (2015) EDDA 1.0: integrated simulation of debris flow erosion, deposition and property changes. Geosci Model Dev 8(3):829–844

Chen Y, Uchimura T, Irfan M, Huang D, Xie J (2017) Detection of water infiltration and deformation of unsaturated soils by elastic wave velocity. Landslides 14(5):1715–1730

Chen Y, Zhou C, Jing L (2009) Modeling coupled THM processes of geological porous media with multiphase flow: theory and validation against laboratory and field scale experiments. Comput Geotech 36(8):1308–1329

Chen YF, Zhou JQ, Hu SH, Hu R, Zhou CB (2015) Evaluation of Forchheimer equation coefficients for non-Darcy flow in deformable rough-walled fractures. J Hydrol 529:993–1006. https://doi.org/10.1016/j.jhydrol.2015.09.021

Chetti A, Benamar A, Hazzab A (2016) Modeling of particle migration in porous media: application to soil suffusion. Transp Porous Med 113(3):591–606

Cho SE, Lee SR (2001) Instability of unsaturated soil slopes due to infiltration. Comput Geotech 28(3):185–208

Cho SE, Lee SR (2002) Evaluation of surficial stability for homogeneous slopes considering rainfall characteristics. J Geotech Geoenviron Eng 128(9):756–763

Chui TM, Freyberg DL (2009) Implementing hydrologic boundary conditions in a multiphysics model. J Hydrol Eng 14(12):1374–1377

Ciervo F, Casini F, Papa MN, Rigon R (2015) Some remarks on bimodality effects of the hydraulic properties on shear strength of unsaturated soils. Vadose Zone J 14(9). https://doi.org/10.2136/vzj2014.10.0152

Cividini A, Bonomi S, Vignati GC, Gioda G (2009) Seepage-induced erosion in granular soil and consequent settlement. Int J Geomech 9(4):187–194

Cividini A, Gioda G (2004) Finite element approach to the erosion and transport of fine particles in granular soils. Int J Geomech 4(3):191–198

COMSOL AB (2010) COMSOL multiphysics modeling guide, version 4.0a. Burlington, MA

Crosta G, di Prisco C (1999) On slope instability induced by seepage erosion. Can Geotech J 36(6):1056–1073

Crosta GB, Frattini P (2003) Distributed modelling of shallow landslides triggered by intense rainfall. Nat Hazards Earth Syst Sci 3(1-2):81–93

Dai FC, Lee CF, Wang SJ (2003) Characterization of rainfall-induced landslides. Int J Remote Sens 24(23):4817–4834

Darby SE, Rinaldi M, Dapporto S (2007) Coupled simulations of fluvial erosion and mass wasting for cohesive river banks. J Geophys Res Atmos 112(F3). https://doi.org/10.1029/ 2006JF000722

Deuflhard P (1974) A modified Newton method for the solution of ill-conditioned systems of nonlinear equations with application to multiple shooting. Numer Math 22(4):289–315

Fannin RJ, Moffat R (2006) Observations on internal stability of cohesionless soils. Géotechnique 56(7):497–500

Fell R, Fry JJ (2007) The state of the art of assessing the likelihood of internal erosion of embankment dams, water retaining structures and their foundations. In: Fell R, Fry JJ (eds) Internal erosion of dams and their foundations. Taylor and Francis, London, pp 1–23

Fell R, Wan CF, Cyganiewicz J, Foster M (2003) Time for development of internal erosion and piping in embankment dams. J Geotech Geoenviron Eng 129(4):307–314

Fourie AB (1996) Predicting rainfall-induced slope instability. Proc Inst Civil Eng Geotech Eng 119(4):211–218

Fox GA, Wilson GV (2010) The role of subsurface flow in hillslope and stream bank erosion: a review. Soil Sci Soc Am J 74(3):717–733

Fredlund DG, Rahardjo H (1993) Soil mechanics for unsaturated soils. Wiley, New York

Fredlund MD, Wilson GW, Fredlund DG (2002) Use of the grain-size distribution for estimation of the soil-water characteristic curve. Can Geotech J 39(5):1103–1117

Fujisawa K, Murakami A, Nishimura S (2010) Numerical analysis of the erosion and the transport of fine particles within soils leading to the piping phenomenon. Soils Found 50(4):471–482

Giuseppe F, Simoni S, Godt JW, Lu N, Rigon R (2016) Geomorphological control on variably saturated hillslope hydrology and slope instability. Water Resour Res 52(6):4590–4607

Glade T, Anderson MG, Crozier MJ (2006) Landslide hazard and risk. Wiley, New York

Govindaraju RS, Reddi LN, Kasavaraju SK (1995) A physically based model for mobilization of kaolinite particles under hydraulic gradients. J Hydrol 172(1-4):331–350

Hanson GJ, Simon A (2001) Erodibility of cohesive streambeds in the loess area of the midwestern USA. Hydrol Process 15(1):23–38

Hindmarsh AC, Brown PN, Grant KE, Lee SL, Serban R, Shumaker DE, Woodward CS (2005) SUNDIALS: suite of nonlinear and differential/algebraic equation solvers. ACM Trans Math Softw 31(3):363–396

Hu MJ, Wang R, Meng QS, Liu GS (2005) Research on erosion process and features of loose gravelly soil slope. Rock Soil Mech 26(11):1722–1726 (in Chinese)

Indraratna B, Nguyen VT, Rujikiatkamjorn C (2011) Assessing the potential of internal erosion and suffusion of granular soils. J Geotech Geoenviron Eng 137(5):550–554

Istomina VS (1957) Filtration stability of soils. Gostroizdat, Moscow, Leningrad (in Russian)

Iverson RM (2000) Landslide triggering by rain infiltration. Water Resour Res 36(7):1897–1910

Jian BT, Lu XB, Wang SY, Chen XQ, Cui P (2005) The movement of fine grains and its effects on the landslide and debris flow caused by raining. Chin J Underg Sp Eng 1(7):1014–1016 (in Chinese)

Johari A, Habibagahi G, Ghahramani A (2006) Prediction of soil-water characteristic curve using genetic programming. J Geotech Geoenviron Eng 132(5):661–665

Kenney TC, Chiu CE, Ofoegbu GI, Omange GN, Ume CA (1985) Controlling constriction sizes of granular filters. Can Geotech J 22(1):32–43

Kenney TC, Lau D (1985) Internal stability of granular filters. Can Geotech J 22(2):215–225

Kezdi A (1969) Increase of protective capacity of flood control dikes. Department of Geotechnique, Technical University, Budapest, Hungary, Report 1 (in Hungarian)

Kozeny J (1927) Ueber kapillare leitung des wassers im boden. Sitzungsber Akad Wiss Wien 136:271–306

Li M, Fannin RJ (2008) Comparison of two criteria for internal stability of granular soil. Can Geotech J 45(9):1303–1309

Li X, Li JH, Zhang LM (2014) Predicting bimodal soil-water characteristic curves and permeability functions using physically based parameters. Comput Geotech 57:85–96. https://doi.org/10.1016/j.compgeo.2014.01.004

Lumb P (1962) Effect of rain storms on slope stability. Proceedings of the Symposium on Hong Kong Soils, Hong Kong, pp 73-87

Mondal S, Mandal S (2017) RS & GIS-based landslide susceptibility mapping of the Balason River basin, Darjeeling Himalaya, using logistic regression (LR) model. Georisk. https://doi.org/10.1080/17499518.2017.1347949

Mualem Y (1976) A new model for predicting the hydraulic conductivity of unsaturated porous media. Water Resour Res 12(3):513–522

Papamichos E, Vardoulakis I (2005) Sand erosion with a porosity diffusion law. Comput Geotech 32(1):47–58

Partheniades E (1965) Erosion and deposition of cohesive soils. J Hydraul Eng Div ASCE 91(HY1):105–139

Peng M, Zhang LM (2012) Breaching parameters of landslide dams. Landslides 9(1):13–31

Salciarini D, Fanelli G, Tamagnini C (2017) A probabilistic model for rainfall-induced shallow landslide prediction at the regional scale. Landslides 14(5):1731–1746

Santoso AM, Phoon KK, Quek ST (2011) Effects of soil spatial variability on rainfall-induced landslides. Comput Struct 89(11-12):893–900

Sato M, Kuwano R (2015) Suffusion and clogging by one-dimensional seepage tests on cohesive soil. Soils Found 55(6):1427–1440

Schuler U (1995) How to deal with the problem of suffosion. In: Research and development in the field of dams. SNCLD, Crans-Montana, Switzerland, pp 145-159

Schuster RL, Highland LM (2007) The third Hans Cloos lecture. Urban landslides: socioeconomic impacts and overview of mitigative strategies. Bull Eng Geol Environ 66(1):1–27

Seghir A, Benamar A, Wang H (2014) Effects of fine particles on the suffusion of cohesionless soils. Experiments and modeling. Transp Porous Med 103(2):233–247

Sidle RC, Ochiai H (2006) Landslides: processes, prediction, and land use. Water Res M 18. American Geophysical Union, Washington, DC

Skempton AW, Brogan JM (1994) Experiments on piping in sandy gravels. Géotechnique 44(3):449–460

Sterpi D (2003) Effects of the erosion and transport of fine particles due to seepage flow. Int J Geomech 3(1):111–122

Tang D, Li DQ, Cao ZJ (2017) Slope stability analysis in the three gorges reservoir area considering effect of antecedent rainfall. Georisk 11(2):161–172

Terzaghi K (1939) Soil mechanics: a new chapter in engineering science. J Inst Civil Eng 12:106–141

Vahedifard F, Sehat S, Aanstoos JV (2017) Effects of rainfall, geomorphological and geometrical variables on vulnerability of the lower Mississippi River levee system to slump slides. Georisk 11(3):257–271

van Genuchten MTH (1980) A close-form equation for predicting the hydraulic conductivity of unsaturated soils. Soil Sci Soc Am J 44:892–898

Vardoulakis I, Stavropoulou M, Papanastasiou P (1996) Hydromechanical aspects of the sand production problem. Transp Porous Media 22(2):225–244

Vereecken H, Weynants M, Javaux M, Pachepsky Y, Schaap MG, Genuchten MT (2010) Using pedotransfer functions to estimate the van Genuchten-Mualem soil hydraulic properties: a review. Vadose Zone J 9(4):795–820

Wan CF, Fell R (2004) Investigation of rate of erosion of soils in embankment dams. J Geotech Geoenviron Eng 130(4):373–380

Wan CF, Fell R (2008) Assessing the potential of internal instability and suffusion in embankment dams and their foundations. J Geotech Geoenviron Eng 134(3):401–407

Wilson GV, Periketi RK, Fox GA, Dabney SM, Shields FD, Cullum RF (2007) Soil properties controlling seepage erosion contributions to streambank failure. Earth Surf Process Landf 32(3):447–459

Wu LZ, Zhang LM (2009) Analytical solution to 1D coupled water infiltration and deformation in unsaturated soils. Int J Numer Anal Methods Geomech 33(6):773–790

Xiong Y, Bao X, Ye B, Zhang F (2014) Soil-water-air fully coupling finite element analysis of slope failure in unsaturated ground. Soils Found 54(3):377–395

Xu Y, Zhang LM (2009) Breaching parameters for earth and rockfill dams. J Geotech Geoenviron Eng 135(12):1957–1970

Ye GL, Zhang F, Yashima A, Sumi T, Ikemura T (2005) Numerical analyses on progressive failure of slope due to heavy rain with 2D and 3D FEM. Soils Found 45(2):1–15

Zhang LL, Fredlund DG, Zhang LM, Tang WH (2004) Numerical study of soil conditions under which matric suction can be maintained. Can Geotech J 41(4):569–582

Zhang LL, Li JH, Li X, Zhang J, Zhu H (2016a) Rainfall-induced soil slope failure stability analysis and probabilistic assessment. CRC Press, Boca Raton

Zhang LM, Chen Q (2005) Predicting bimodal soil-water characteristic curves. J Geotech Geoenviron Eng 131(5):666–670

Zhang LM, Chen Q (2006) Analysis of seepage failure of the Gouhou rockfill dam during reservoir water infiltration. Soils Found 46(5):557–568

Zhang LM, Peng M, Chang DS, Xu Y (2016b) Dam failure mechanisms and risk assessment. Wiley, London